

Multi-dimension SVPWM-based sensorless control of 7-phase PMSM drives

Kamel Saleh¹, Mark Sumner²

¹Department of Electrical Engineering, Faculty of Engineering, An-Najah National University, Nablus, Palestine

²Department of Electrical and Electronic Engineering, College of Engineering, University of Nottingham, Nottingham, United Kingdom

Article Info

Article history:

Received Aug 28, 2022

Revised Oct 24, 2022

Accepted Nov 2, 2022

Keywords:

7-phase motor

Multi-dimension SVPWM

Sensorless

ABSTRACT

A new control technique for the 7-phase permanent magnet synchronous machine (PMSM) when a failure in the speed sensor is introduced. This will make the whole drive system more robust and at the same time reduce the cost. The speed and the position of the shaft of the motor are obtained by tracking the saturation saliency of the 7-phase motor when a failure in speed sensor is occurred. The proposed saliency-tracking algorithm is based on measuring the derivative of the stator currents of the 7-phase motor after the switching of the insulated gate bipolar transistor (IGBT) of the 7-phase inverter due to the implementation of the multi-dimension space vector pulse width modulation (SVPWM). This modulation technique is used in the 7-phase drives to suppress the 3rd and 5th harmonics. Simulation results show that the 7-phase motor drive could track the reference speed at different load conditions when a failure in the speed sensor is occurred without compromising the performance.

This is an open access article under the [CC BY-SA](https://creativecommons.org/licenses/by-sa/4.0/) license.



Corresponding Author:

Kamel Saleh

Department of Electrical and Electronic Engineering, Faculty of Engineering

An-Najah National University

Nablus, Palestine

Email: kamel.saleh@najah.edu

1. INTRODUCTION

Multi-phase motors have gained significant interest in research in the new century [1], [2]. The benefits of these machines are what have sparked this interest. These benefits including high power, low torque ripple, and most importantly, good performance under fault conditions. The space vector pulse width modulation (SVPWM) technique can be utilized in the multi-phase drive system too with some extensions to consider the increased number of the switching vectors and the existence of 3rd, 5th and other harmonics. These SVPWM techniques are called multi-dimension SVPWM that will produce a sinusoidal output voltage by synthesizing voltage vectors in several d-q subspaces [3]–[9].

Industrial drive systems predominately use speed-controlled systems. These speed-controlled drives are based on vector control theory where the d-q components of the stator current are acquired using the rotor position determined by optical encoders or resolvers. However, utilizing such sensors will decrease the overall reliability of the drive system. Therefore, much research is directed toward “sensorless” or “encoderless” vector control where the rotor position is obtained without using the speed sensors [10]–[15].

Speed control of the 5-phase motor when a failure in the speed sensor is occurred has been researched in many papers published in the last decade. Some of these papers used were model-based techniques. Others used the direct-torque control method to obtain a speed-controlled the 5-phase motor. And few papers used a high-frequency injection method to get the speed and position of the 5-phase motor [16]–[20]. In the past

couple of years, a few papers have been published in the field of the model-based sensorless control of the 7-phase motor [21]–[27]. In this year, a new paper has been published in the field of sensorless control of the 7-phase motor based on voltage excitation when a failure in the speed sensor is occurred [28]. The paper has compared three techniques to track the saliency of the 7-phase drive in terms of the current distortion. Although the three algorithms presented in that paper and the algorithm presented in this paper are using the same technique to get the shaft speed and position when a failure in the speed sensor is occurred, there are two major differences. The first one is the algorithm presented in this paper is much easier to be implemented than the algorithms presented in that paper. The second difference is that the algorithm presented in this paper to track the saturation saliency isn't needing any offline commissioning to achieve a closed-loop sensorless speed control while the algorithms presented in that paper need a lot of offline commissioning effort. This is because the DC offset of all the saturation saliency position scalars is equal in the new algorithm in all sectors while the dc offset of the position scalars is different in the same sector and between sectors. Finally, the new algorithm can be applied to acquire the saliency position in the 7-phase motor drives when one phase of the motor is lost due to the open-circuit failure while the algorithms published in [28] can't.

This research is presenting a speed control of the 7-phase drive based on the voltage excitation method when a failure in speed sensor is occurred. This will make the whole drive system more robust and reduce the cost. The voltage excitation technique is a technique used to get shaft speed and position through tracking the saliency. The tracking of the saliency is relying on measuring the current derivative of the stator motor currents when the insulated gate bipolar transistor (IGBT) of the inverter are switched on and off resulted by implementing the multi-dimension SVPWM used in a 7-phase motor.

2. OPERATION OF THE 7-PHASE PMSM WITHOUT FAULT

2.1. Modelling the 7-phase PMSM

Figure 1 demonstrates the 7-phase permanent magnet synchronous machine (PMSM) drive topology. The 7-phase motor is fed from the 7-phase inverter. The IGBTs in the 7-phase inverter will be switched according to the pulse width modulation (PWM) signals generated using the multi-dimension SVPWM technique. The details of the multi-dimension SVPWM will be discussed in section 2.2. The model of the 7-phase drive is given in (1)-(3).

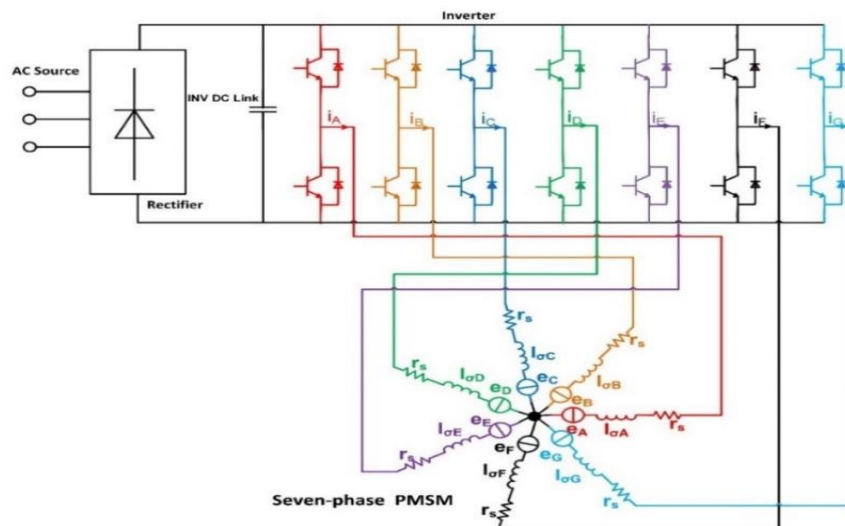


Figure 1. 7-phase drive topology

$$[V_s] = r_s * [I_s] + q * [\varphi_s] \tag{1}$$

Where $[V_s] = [V_{sA}, V_{sB}, V_{sC}, V_{sD}, V_{sE}, V_{sF}, V_{sG}]^T$ are the stator applied voltages, r_s is the stator resistance, $[I_s] = [i_{sA}, i_{sB}, i_{sC}, i_{sD}, i_{sE}, i_{sF}, i_{sG}]^T$ are the stator currents, $q = \frac{d}{dt}$ and $[\varphi_s] = [\varphi_{sA}, \varphi_{sB}, \varphi_{sC}, \varphi_{sD}, \varphi_{sE}, \varphi_{sF}, \varphi_{sG}]^T$ are the stator linkage fluxes. The stator linkage fluxes can be expressed as in (2).

$$[\varphi_s] = L_s * [I_s] + \varphi_M \tag{2}$$

$$\varphi_M = \lambda_m * \begin{bmatrix} \cos(\theta_R) \\ \cos(\theta_R - 2\theta_x) \\ \cos(\theta_R - 4\theta_x) \\ \cos(\theta_R - 6\theta_x) \\ \cos(\theta_R - 8\theta_x) \\ \cos(\theta_R - 10\theta_x) \\ \cos(\theta_R - 12\theta_x) \end{bmatrix} \tag{3}$$

Where L_s is the stator inductances matrix, λ_m is the peak permanent magnet flux linkage, θ_R is the rotor position, and θ_x is $\pi/7$. The parameters of the motor that is used in this research are as following: rated voltage=400 V, rated speed=1500 rpm, rated torque=12 N.m, rated power=2.15 kW, $k_t=1.2$ N.m/A, $k_e=147$ v/Krpm, inertia=20kg/cm², R(ph-ph)=4 Ω , and L(ph-ph)=29.8 mH.

2.2. Multi-dimension SVPWM technique

2.2.1. Space vectors distribution

It is well known that if the output voltage of the inverter has any 3rd or 5th harmonics, then this will produce a large 3rd and 5th harmonics in the 7-phase motor currents. The reason for that is these harmonics will be limited by the stator impedances only [3]–[8] as no rotating MMF is produced. Therefore, it is crucial to remove the third and fifth harmonics from the inverter's output voltage in a 7-phase motor drive. This can be achieved by extracting these components and then controlling them to be zero. To extract the 3rd and 5th harmonics from the fundamental component, the reference voltage (V_{ref}) is needed to be decoupled into three planes. The first plan is rotating at a synchronous speed called the $\alpha 1$ - $\beta 1$ plane to extract the fundamental V_{ref} . The second one is rotating 3 times faster than the first plane called the $\alpha 3$ - $\beta 3$ plane to extract the 3rd harmonic. The final one is rotating 5 times faster than the first plane called the $\alpha 5$ - $\beta 5$ plane to extract the 5th harmonic component of the V_{ref} using the transformation given in (4)-(6).

$$\begin{bmatrix} \alpha 1 \\ \beta 1 \\ \alpha 3 \\ \beta 3 \\ \alpha 5 \\ \beta 5 \end{bmatrix} = [G] \begin{bmatrix} A \\ B \\ C \\ D \\ E \\ F \\ G \end{bmatrix} \tag{4}$$

$$\begin{bmatrix} A \\ B \\ C \\ D \\ E \\ F \\ G \end{bmatrix} = [G^{-1}] \begin{bmatrix} \alpha 1 \\ \beta 1 \\ \alpha 3 \\ \beta 3 \\ \alpha 5 \\ \beta 5 \end{bmatrix} \tag{5}$$

where

$$G = \frac{1}{2} \begin{bmatrix} 1 & \cos(2\theta_x) & \cos(4\theta_x) & \cos(6\theta_x) & \cos(8\theta_x) & \cos(10\theta_x) & \cos(12\theta_x) \\ 0 & \sin(2\theta_x) & \sin(4\theta_x) & \sin(6\theta_x) & \sin(8\theta_x) & \sin(10\theta_x) & \sin(12\theta_x) \\ 1 & \cos 6(\theta_x) & \cos 12(\theta_x) & \cos 18(\theta_x) & \cos 24(\theta_x) & \cos 30(\theta_x) & \cos 36(\theta_x) \\ 0 & \sin 6(\theta_x) & \sin 12(\theta_x) & \sin 18(\theta_x) & \sin 24(\theta_x) & \sin 30(\theta_x) & \sin 36(\theta_x) \\ 1 & \cos 10(\theta_x) & \cos 20(\theta_x) & \cos 30(\theta_x) & \cos 40(\theta_x) & \cos 50(\theta_x) & \cos 60(\theta_x) \\ 0 & \sin 10(\theta_x) & \sin 20(\theta_x) & \sin 30(\theta_x) & \sin 40(\theta_x) & \sin 50(\theta_x) & \sin 60(\theta_x) \end{bmatrix} \tag{6}$$

By utilizing the zero-sequence voltage, the vectors V_{s1} , V_{s3} , and V_{s5} in the $\alpha 1$ - $\beta 1$, $\alpha 3$ - $\beta 3$, and $\alpha 5$ - $\beta 5$ planes respectively can be deduced directly using (7).

$$\begin{bmatrix} V_{s1} \\ V_{s3} \\ V_{s5} \end{bmatrix} = \frac{2}{7} \times V_{DC} \times \begin{bmatrix} 1 & e^{2j\theta_x} & e^{4j\theta_x} & e^{6j\theta_x} & e^{8j\theta_x} & e^{10j\theta_x} & e^{12j\theta_x} \\ 1 & e^{3 \times 6j\theta_x} & e^{3 \times 4j\theta_x} & e^{3 \times 6j\theta_x} & e^{3 \times 8j\theta_x} & e^{3 \times 10j\theta_x} & e^{3 \times 12j\theta_x} \\ 1 & e^{5 \times 2j\theta_x} & e^{5 \times 4j\theta_x} & e^{5 \times 6j\theta_x} & e^{5 \times 8j\theta_x} & e^{5 \times 10j\theta_x} & e^{5 \times 12j\theta_x} \end{bmatrix} \begin{bmatrix} S_A \\ S_B \\ S_C \\ S_D \\ S_E \\ S_F \\ S_G \end{bmatrix} \tag{7}$$

Where V_{DC} is the DC link voltage, and $S_A, S_B, S_C, S_D, S_E, S_F,$ and S_G are the pulses to trigger the upper IGBTs of the 7-phase inverter. Based in (7), a 128-switching vector can be generated and distributed in space as shown in Figures 2, 3(a) and (b). The amplitude of the vectors U1-U7 are given in Table 1.

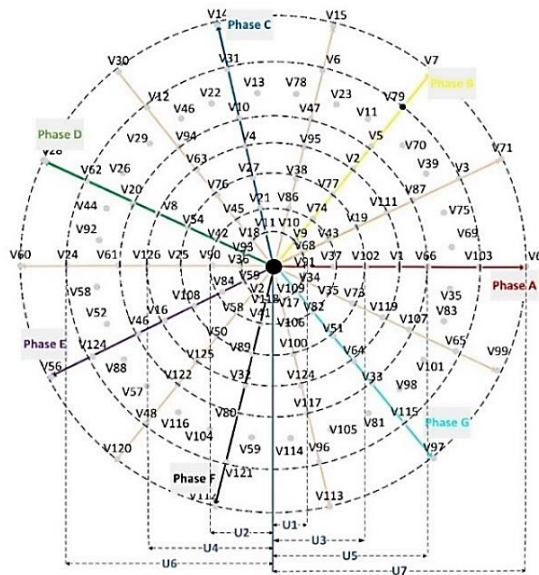


Figure 2. Voltage vector space distribution in α_1 - β_1 plan

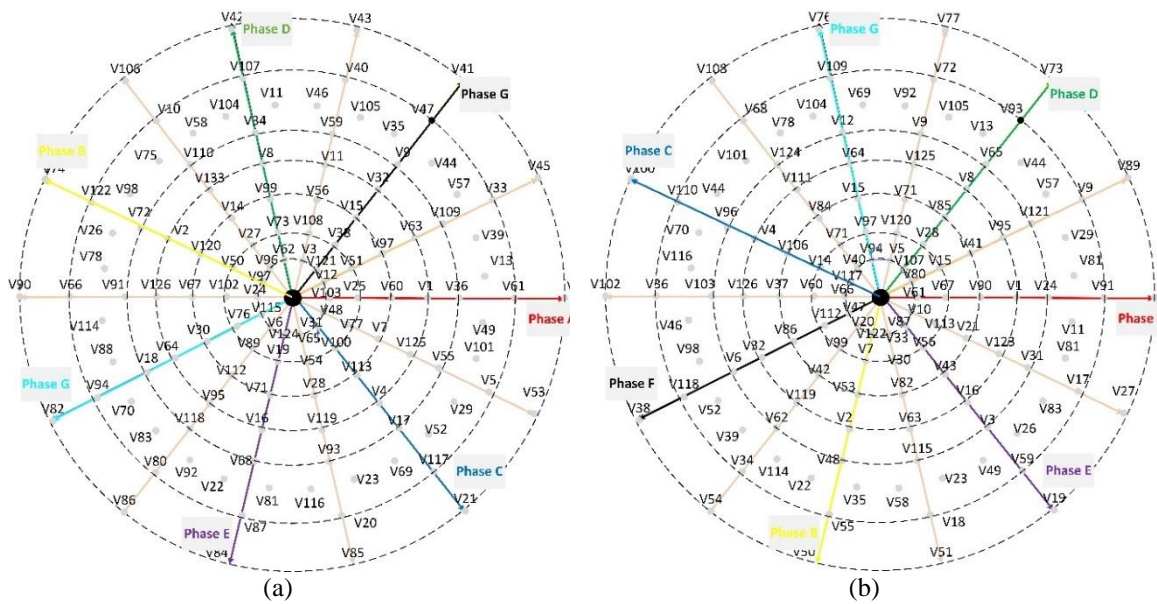


Figure 3. Voltage vector space distribution in (a) α_3 - β_3 plan and (b) α_5 - β_5 plan

Table 1. Switching vector amplitudes

Vector group name	U1	U2	U3	U4	U5	U6	U7
Amplitude	$0.127 \times V_{DC}$	$0.159 \times V_{DC}$	$0.229 \times V_{DC}$	$0.286 \times V_{DC}$	$0.356 \times V_{DC}$	$0.515 \times V_{DC}$	$0.642 \times V_{DC}$

2.2.2. Switching vector selection and dwell time calculation

Theoretically, the seven vector groups (U1, U2, U3, U4, U5, U6, and U7) can be utilized to synthesize the V_{ref} . But, only the adjacent vectors U4, U6, and U7 are utilized to generate the V_{ref} in each sector practically. This is related to the non-continuity and the modest amplitude of the vectors U1, U2, U3, and U5. For instance, the six active vectors V1 (1000000), V3 (1100000), V67(1100001), V71(1110001),

V103(1110011), V111(1111011) in addition to the two null vectors V0(0000000), and V127(1111011) are utilized to generate the V_ref in sector 1 in $\alpha 1-\beta 1$, $\alpha 3-\beta 3$, and $\alpha 5-\beta 5$ planes respectively as illustrated in Figures 4(a)-(c) respectively. The associated SVPWM waveform is depicted in Figure 4(d). The time of application of each vector is derived as (8).

$$\begin{bmatrix} T_1 \\ T_2 \\ T_3 \\ T_4 \\ T_5 \\ T_6 \end{bmatrix} = T_s \times [T^{-1}] \begin{bmatrix} V_{ref_ \alpha 1} \\ V_{ref_ \beta 1} \\ V_{ref_ \alpha 3} \\ V_{ref_ \beta 3} \\ V_{ref_ \alpha 5} \\ V_{ref_ \beta 5} \end{bmatrix} \tag{8}$$

$$T = \begin{bmatrix} U4 & U6\cos(\theta_x) & U7 & U7\cos(\theta_x) & U6 & U4\cos(\theta_x) \\ 0 & U6\sin(\theta_x) & 0 & U7\sin(\theta_x) & 0 & U4\sin(\theta_x) \\ U4 & U1\cos(3\theta_x) & -U3 & U3\cos(10\theta_x) & U1 & U4\cos(3\theta_x) \\ 0 & U1\sin(3\theta_x) & 0 & U3\sin(10\theta_x) & 0 & U4\sin(3\theta_x) \\ U4 & U5\cos(12\theta_x) & U2 & U2\cos(5\theta_x) & -U5 & U4\cos(5\theta_x) \\ 0 & U5\sin(12\theta_x) & 0 & U2\sin(5\theta_x) & 0 & U4\sin(5\theta_x) \end{bmatrix} \tag{9}$$

where

$$T_0 = T_s - T_1 - T_2 - T_3 - T_4 - T_5 - T_6 \tag{10}$$

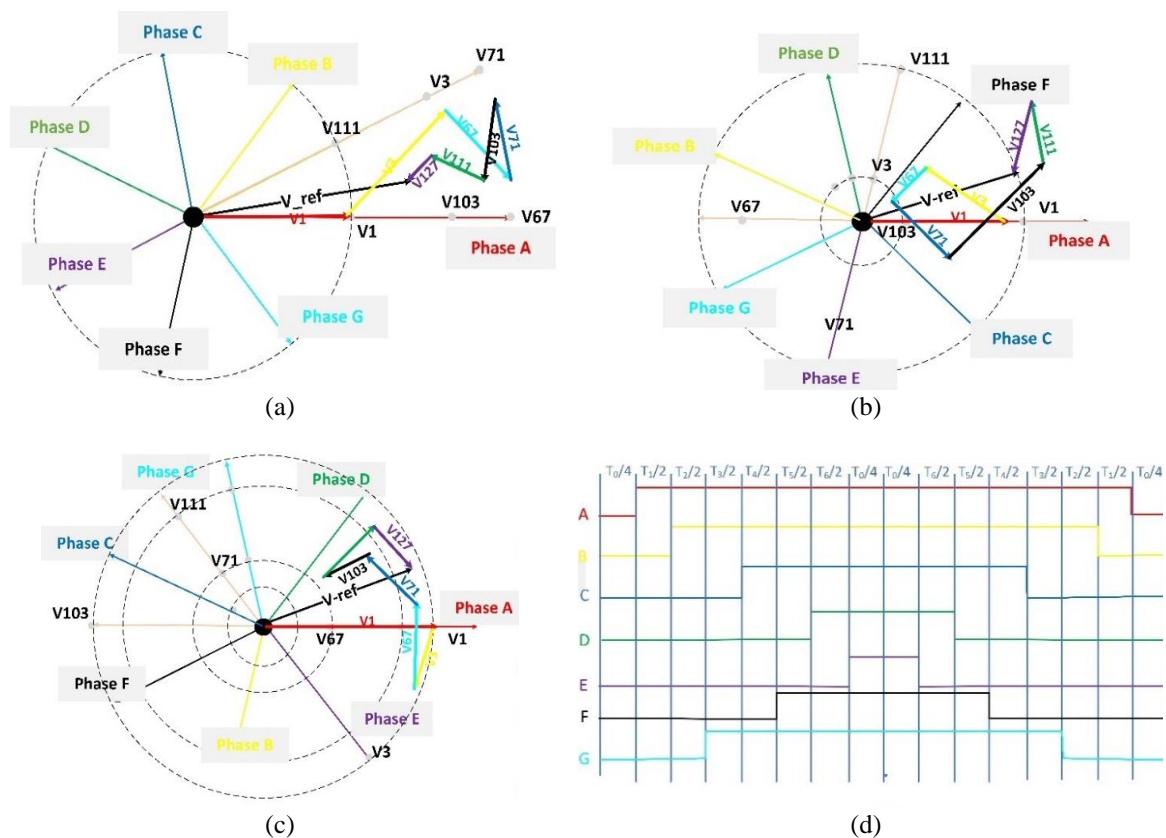


Figure 4. Multi-dimension SVPWM vector synthesis in; (a) $\alpha 1 - \beta 1$ plan, (b) $\alpha 3 - \beta 3$ plan, (c) $\alpha 5 - \beta 5$ plan, and (d) NSV-SVPWM waveform

The algorithm to implement the multi-dimension SVPWM in terms of calculating the dwell time and the switching sequence in any sector k is given in the flow chart shown in Figure 5. Table 2 in addition to w1 and w2 are shown below.

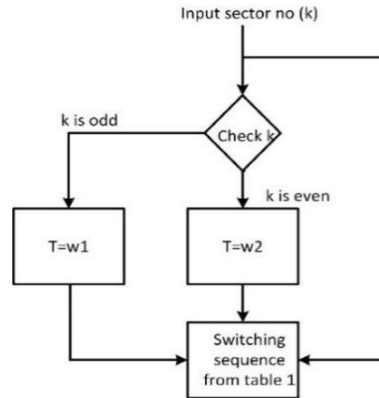


Figure 5. Multi-dimension implementation algorithm

Table 2. switching sequence in different sectors using multi-dimension SVPWM

Sector no	H0	H1	H2	H3	H4	H5	H6	H7
1	V0 (0000000)	V1 (1000000)	V3 (1100000)	V67 (1100001)	V71 (1110001)	V103 (1110011)	V111 (1111011)	V127 (1111111)
2	V0 (0000000)	V2 (0100000)	V3 (1100000)	V7 (1110000)	V71 (1110001)	V79 (1111001)	V111 (1111011)	V127 (1111111)
3	V0 (0000000)	V2 (0100000)	V6 (0110000)	V7 (1110000)	V15 (1111000)	V79 (1111001)	V95 (1111101)	V127 (1111111)
4	V0 (0000000)	V4 (0100000)	V6 (0110000)	V14 (0111000)	V15 (1111000)	V31 (1111100)	V95 (1111101)	V127 (1111111)
5	V0 (0000000)	V4 (0100000)	V12 (0110000)	V14 (0111000)	V30 (1111100)	V31 (1111100)	V63 (1111110)	V127 (1111111)
6	V0 (0000000)	V8 (0010000)	V12 (0011000)	V28 (0111000)	V30 (1111100)	V62 (1111110)	V63 (1111110)	V127 (1111111)
7	V0 (0000000)	V8 (0010000)	V24 (0011000)	V28 (0111000)	V60 (0111100)	V62 (1111110)	V126 (1111110)	V127 (1111111)
8	V0 (0000000)	V16 (0001000)	V24 (0001100)	V56 (0011100)	V60 (1001110)	V124 (0111111)	V126 (1111111)	V127 (1111111)
9	V0 (0000000)	V16 (0001000)	V48 (0001100)	V56 (0001110)	V120 (0011110)	V124 (0111111)	V125 (1011111)	V127 (1111111)
10	V0 (0000000)	V32 (0000100)	V48 (0000110)	V112 (0000111)	V120 (0001111)	V121 (1001111)	V125 (1011111)	V127 (1111111)
11	V0 (0000000)	V32 (0000100)	V96 (0000111)	V112 (0000111)	V113 (1000111)	V121 (1001111)	V124 (1101111)	V127 (1111111)
12	V0 (0000000)	V64 (0000010)	V96 (0000011)	V97 (1000011)	V113 (1000111)	V115 (1100111)	V124 (1101111)	V127 (1111111)
13	V0 (0000000)	V64 (0000010)	V65 (1000011)	V97 (1000011)	V99 (1100011)	V115 (1100111)	V119 (1110111)	V127 (1111111)
14	V0 (0000000)	V1 (1000000)	V65 (1000001)	V67 (1100001)	V99 (1100011)	V103 (1110011)	V119 (1110111)	V127 (1111111)

$$w1 = \begin{bmatrix} U4 \times \cos((k-1)\theta_x) & U6 \times \cos(k\theta_x) & U7 \times \cos((k-1)\theta_x) & U7 \times \cos(k\theta_x) & U6 \times \cos((k-1)\theta_x) & U4 \times \cos(k\theta_x) \\ U4 \times \sin((k-1)\theta_x) & U6 \times \sin(k\theta_x) & U7 \times \sin((k-1)\theta_x) & U7 \times \sin(k\theta_x) & U6 \times \sin((k-1)\theta_x) & U4 \times \sin(k\theta_x) \\ U4 \times \cos(3(k-1)\theta_x) & U1 \times \cos(3k\theta_x) & -U3 \times \cos(3(k-1)\theta_x) & -U3 \times \cos(3k\theta_x) & U1 \times \cos(3(k-1)\theta_x) & U4 \times \cos(3k\theta_x) \\ U4 \times \sin(3(k-1)\theta_x) & U1 \times \sin(3k\theta_x) & -U3 \times \sin(3(k-1)\theta_x) & -U3 \times \sin(3k\theta_x) & U1 \times \sin(3(k-1)\theta_x) & U4 \times \sin(3k\theta_x) \\ U4 \times \cos(5(k-1)\theta_x) & -U5 \times \cos(5k\theta_x) & U2 \times \cos(5(k-1)\theta_x) & U2 \times \cos(5k\theta_x) & -U5 \times \cos(5(k-1)\theta_x) & U4 \times \cos(5k\theta_x) \\ U4 \times \sin(5(k-1)\theta_x) & -U5 \times \sin(5k\theta_x) & U2 \times \sin(5(k-1)\theta_x) & U2 \times \sin(5k\theta_x) & -U5 \times \sin(5(k-1)\theta_x) & U4 \times \sin(5k\theta_x) \end{bmatrix}$$

$$w2 = \begin{bmatrix} U4 \times \cos(k\theta_x) & U6 \times \cos((k-1)\theta_x) & U7 \times \cos(k\theta_x) & U7 \times \cos((k-1)\theta_x) & U6 \times \cos(k\theta_x) & U4 \times \cos((k-1)\theta_x) \\ U4 \times \sin(k\theta_x) & U6 \times \sin((k-1)\theta_x) & U7 \times \sin(k\theta_x) & U7 \times \sin((k-1)\theta_x) & U6 \times \sin(k\theta_x) & U4 \times \sin((k-1)\theta_x) \\ U4 \times \cos(3k\theta_x) & U1 \times \cos(3(k-1)\theta_x) & -U3 \times \cos(3k\theta_x) & -U3 \times \cos(3(k-1)\theta_x) & U1 \times \cos(3k\theta_x) & U4 \times \cos(3(k-1)\theta_x) \\ U4 \times \sin(3k\theta_x) & U1 \times \sin(3(k-1)\theta_x) & -U3 \times \sin(3k\theta_x) & -U3 \times \sin(3(k-1)\theta_x) & U1 \times \sin(3k\theta_x) & U4 \times \sin(3(k-1)\theta_x) \\ U4 \times \cos(5k\theta_x) & -U5 \times \cos(5(k-1)\theta_x) & U2 \times \cos(5k\theta_x) & U2 \times \cos(5(k-1)\theta_x) & -U5 \times \cos(5k\theta_x) & U4 \times \cos(5(k-1)\theta_x) \\ U4 \times \sin(5k\theta_x) & -U5 \times \sin(5(k-1)\theta_x) & U2 \times \sin(5k\theta_x) & U2 \times \sin(5(k-1)\theta_x) & -U5 \times \sin(5k\theta_x) & U4 \times \sin(5(k-1)\theta_x) \end{bmatrix}$$

2.3. Control of the 7-phase drive without fault

Figure 6 demonstrates the schematic of the vector-control structure that was utilized to achieve a speed-controlled of the 7-phase PMSM drive under healthy operating conditions. It can be noticed from the

figure that rotor position and speed are obtained by the encoder. Moreover, it can be noticed that both the 3rd harmonic and the 5th harmonic components were regulated to zero through putting i_{d3_ref} , i_{q3_ref} , i_{d5_ref} , and i_{q5_ref} to zero. The whole control structure illustrated in Figure 6 was implemented using the SABER simulation package and the results are shown in Figure 7. The speed of the motor was regulated at 180 rpm at half load. The stator currents were symmetrical and shifted by $(\pi/7)$. Moreover, the spectrum of one phase of the motor shows that third 3rd and 5th harmonics were not found as they are regulated to zero. At $t=1.5$ s, the reference speed of the motor was changed to zero rpm. Then at $t=3$ s, the reference speed of the motor was changed back to 180 rpm. In both cases, the system drive has a very good dynamic and transient response.

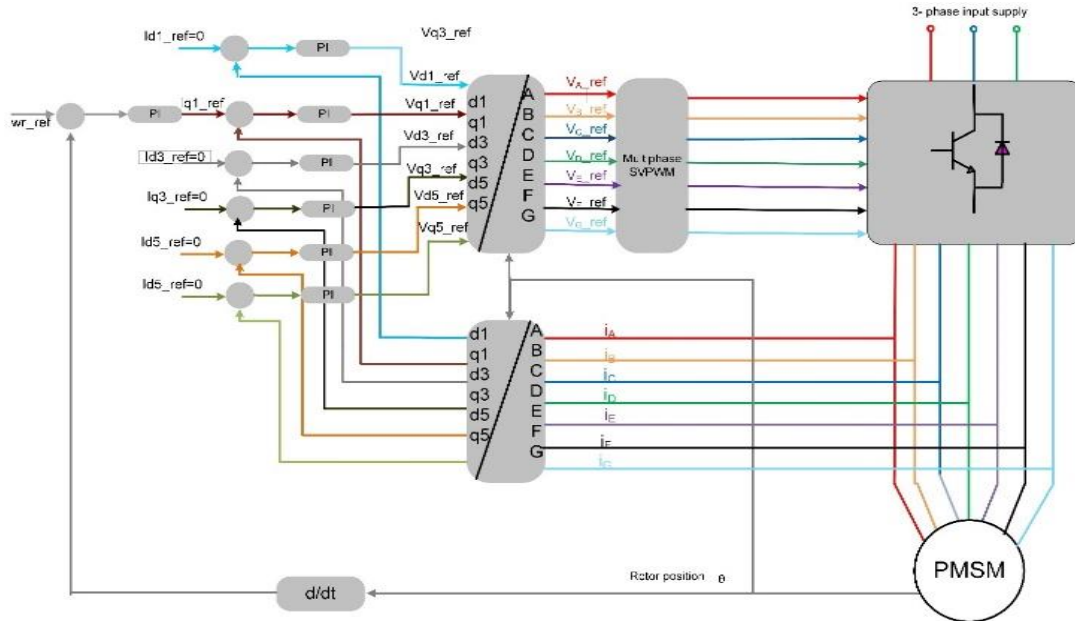


Figure 6. 7-phase drive control structure using multi-dimension SVPWM before speed sensor failure

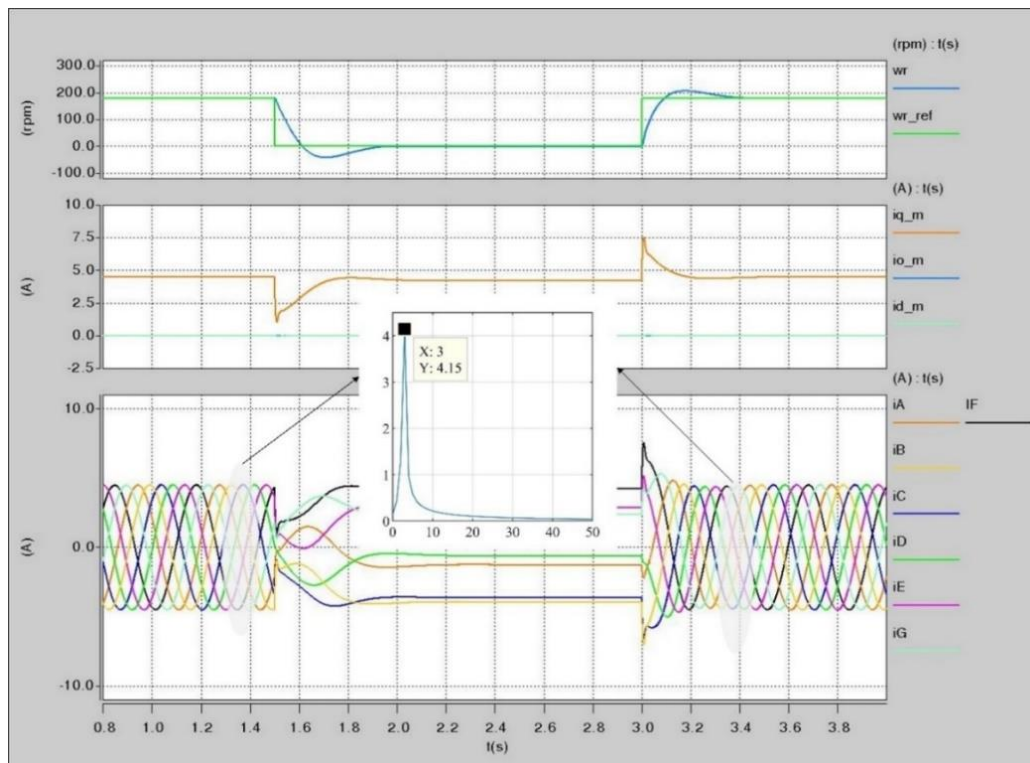


Figure 7. Speed control of the 7- phase motor without faults

3. CONTROL OF THE 7-PHASE PMSM WHEN A FAILURE IN THE SPEED SENSOR IS OCCURRED

3.1. Saliency tracking algorithm

The stator inductance matrix L_s in (2) was modeled to include the effect of the saturation saliency of main flux and hence the term $(2\theta_r)$ was used. Hence, the saliency position and the shaft position can be identified by metering the derivative of the stator currents when the IGBTs are switched on and off in one PWM waveform. Figure 8(a) shows multi-dimension SVPWM vector synthesis and Figure 8(b) shows the PWM waveform for a 7-phase inverter when the V_{ref} exists in sector 1. Also, the figure shows the time instants for metering derivative of the stator current when the inverter IGBTs are switched. The stator circuit when the vectors (H0-H7) i.e (V0, V1, V3, V67, V71, V103, V111, and V127) are applied are shown in Figures 9(a)-(g) respectively.

Using the dynamic equivalent circuit shown in Figure 9(a), (11) holds true.

$$[0] = r_s * [i_{sA}^{(V0)}] + [l_{\sigma sA} * q(i_{sA}^{(V0)})] + [e_{sA}^{(V0)}] \quad (11)$$

Where $l_{\sigma A}$ are the stator leakage inductance in phase 'A' and e_A are the back emf in phase 'A'. Also, (12) is obtained using Figure 9(b).

$$\begin{bmatrix} VDC \\ 0 \end{bmatrix} = r_s * \begin{bmatrix} i_{sA}^{(V1)} \\ i_{sB}^{(V1)} \end{bmatrix} + \begin{bmatrix} l_{\sigma sA} * q(i_{sA}^{(V1)}) \\ l_{\sigma sB} * q(i_{sB}^{(V1)}) \end{bmatrix} + \begin{bmatrix} e_{sA}^{(V1)} \\ e_{sB}^{(V1)} \end{bmatrix} \quad (12)$$

when the dynamic circuit in Figure 9(c) is considered, (13) holds true.

$$\begin{bmatrix} VDC \\ 0 \end{bmatrix} = r_s * \begin{bmatrix} i_{sB}^{(V3)} \\ i_{sG}^{(V3)} \end{bmatrix} + \begin{bmatrix} l_{\sigma sB} * q(i_{sB}^{(V3)}) \\ l_{\sigma sG} * q(i_{sG}^{(V3)}) \end{bmatrix} + \begin{bmatrix} e_{sB}^{(V3)} \\ e_{sG}^{(V3)} \end{bmatrix} \quad (13)$$

Moreover, (14) is obtained using Figure 9(d).

$$\begin{bmatrix} VDC \\ 0 \end{bmatrix} = r_s * \begin{bmatrix} i_{sG}^{(V67)} \\ i_{sC}^{(V67)} \end{bmatrix} + \begin{bmatrix} l_{\sigma sG} * q(i_{sG}^{(V67)}) \\ l_{\sigma sC} * q(i_{sC}^{(V67)}) \end{bmatrix} + \begin{bmatrix} e_{sG}^{(V67)} \\ e_{sC}^{(V67)} \end{bmatrix} \quad (14)$$

When the dynamic circuit in Figure 9(e) is considered, (15) can be derived.

$$\begin{bmatrix} VDC \\ 0 \end{bmatrix} = r_s * \begin{bmatrix} i_{sC}^{(V71)} \\ i_{sF}^{(V71)} \end{bmatrix} + \begin{bmatrix} l_{\sigma sC} * q(i_{sC}^{(V71)}) \\ l_{\sigma sF} * q(i_{sF}^{(V71)}) \end{bmatrix} + \begin{bmatrix} e_{sC}^{(V71)} \\ e_{sF}^{(V71)} \end{bmatrix} \quad (15)$$

Also, when the dynamic circuit in Figure 9(f) is considered, (16) can be derived.

$$\begin{bmatrix} VDC \\ 0 \end{bmatrix} = r_s * \begin{bmatrix} i_{sF}^{(V103)} \\ i_{sD}^{(V103)} \end{bmatrix} + \begin{bmatrix} l_{\sigma sF} * q(i_{sF}^{(V103)}) \\ l_{\sigma sD} * q(i_{sD}^{(V103)}) \end{bmatrix} + \begin{bmatrix} e_{sF}^{(V103)} \\ e_{sD}^{(V103)} \end{bmatrix} \quad (16)$$

Moreover, (17) is obtained using Figure 9(g).

$$\begin{bmatrix} VDC \\ 0 \end{bmatrix} = r_s * \begin{bmatrix} i_{sD}^{(V111)} \\ i_{sE}^{(V111)} \end{bmatrix} + \begin{bmatrix} l_{\sigma sD} * q(i_{sD}^{(V111)}) \\ l_{\sigma sE} * q(i_{sE}^{(V111)}) \end{bmatrix} + \begin{bmatrix} e_{sD}^{(V111)} \\ e_{sE}^{(V111)} \end{bmatrix} \quad (17)$$

Finally, (18) is obtained using Figure 9(h).

$$[VDC] = r_s * [i_{sE}^{(V127)}] + [l_{\sigma sE} * q(i_{sE}^{(V127)})] + [e_{sE}^{(V127)}] \quad (18)$$

By subtracting every two adjacent equations from each other in addition to neglecting the drop voltage on the r_s as it will very small quantity and neglecting the back emf as there will be little change on it (19) can be derived.

$$\begin{bmatrix} \text{VDC} \\ \text{VDC} \\ \text{VDC} \\ \text{VDC} \\ \text{VDC} \\ \text{VDC} \\ \text{VDC} \end{bmatrix} = s \begin{bmatrix} l_{\sigma sA} \times q(i_{sA}^{(V1)} - i_{sA}^{(V0)}) \\ l_{\sigma sB} \times q(i_{sB}^{(V3)} - i_{sB}^{(V1)}) \\ l_{\sigma sC} \times q(i_{sC}^{(V71)} - i_{sC}^{(V67)}) \\ l_{\sigma sD} \times q(i_{sD}^{(V111)} - i_{sD}^{(V103)}) \\ l_{\sigma sE} \times q(i_{sE}^{(V127)} - i_{sE}^{(V111)}) \\ l_{\sigma sF} \times q(i_{sF}^{(V103)} - i_{sF}^{(V71)}) \\ l_{\sigma sG} \times q(i_{sG}^{(V67)} - i_{sG}^{(V3)}) \end{bmatrix} \quad (19)$$

The position scalars $P_{sA}, P_{sB}, P_{sC}, P_{sD}, P_{sE}, P_{sF}$, and P_{sG} can be constructed as given in (20).

$$\begin{bmatrix} P_{sA} \\ P_{sB} \\ P_{sC} \\ P_{sD} \\ P_{sE} \\ P_{sF} \\ P_{sG} \end{bmatrix} = C \times \begin{bmatrix} q(i_{sA}^{(V1)} - i_{sA}^{(V0)}) \\ q(i_{sB}^{(V3)} - i_{sB}^{(V1)}) \\ q(i_{sC}^{(V71)} - i_{sC}^{(V67)}) \\ q(i_{sD}^{(V111)} - i_{sD}^{(V103)}) \\ q(i_{sE}^{(V127)} - i_{sE}^{(V111)}) \\ q(i_{sF}^{(V103)} - i_{sF}^{(V71)}) \\ q(i_{sG}^{(V67)} - i_{sG}^{(V3)}) \end{bmatrix} = C \times \begin{bmatrix} q(i_{sA}^{H1} - i_{sA}^{H0}) \\ q(i_{sB}^{H2} - i_{sB}^{H1}) \\ q(i_{sC}^{H4} - i_{sC}^{H3}) \\ q(i_{sD}^{H6} - i_{sD}^{H5}) \\ q(i_{sE}^{H7} - i_{sE}^{H6}) \\ q(i_{sF}^{H5} - i_{sF}^{H4}) \\ q(i_{sG}^{H3} - i_{sG}^{H2}) \end{bmatrix} \quad (20)$$

where

$$C = \frac{VDC - L_{s0} + L_{s1}}{L_x} \quad (21)$$

To obtain the position signals in all sectors when a failure in the speed sensor is occurred in all sectors, Table 3 can be utilized. These position scalars can be utilized to generate $Palfa, Pbeta$ as (22).

$$\begin{bmatrix} Palfa \\ Pbeta \end{bmatrix} = [V] \begin{bmatrix} P_A \\ P_B \\ P_C \\ P_D \\ P_E \\ P_F \\ P_G \end{bmatrix} \quad (22)$$

where

$$V = \begin{bmatrix} 1 & \cos 4\theta_x & \cos 8\theta_x & \cos 12\theta_x & \cos 2\theta_x & \cos 6\theta_x & \cos 10\theta_x \\ 1 & \sin 4\theta_x & \sin 8\theta_x & \sin 12\theta_x & \sin 2\theta_x & \sin 6\theta_x & \sin 10\theta_x \end{bmatrix} \quad (23)$$

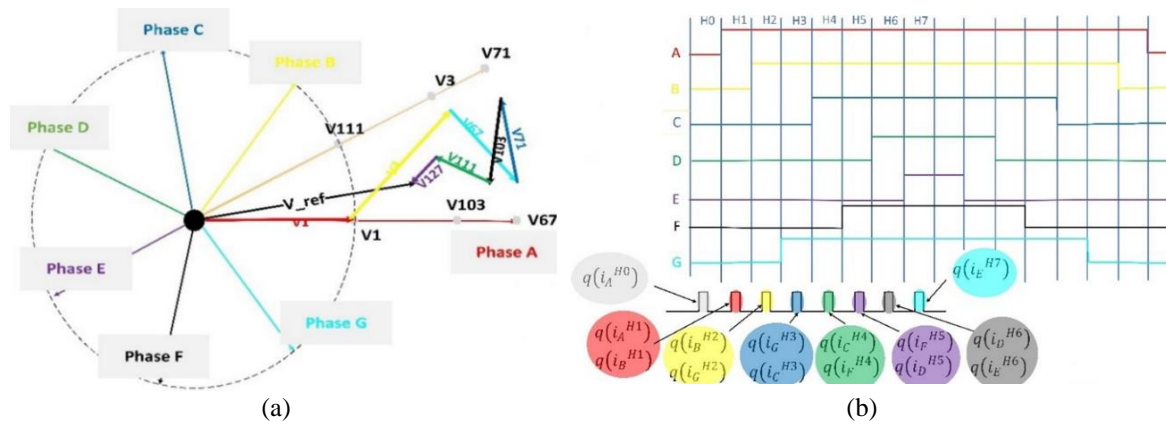


Figure 8. NSV-SVPWM technique; (a) multi-dimension SVPWM vector synthesis and (b) the PWM waveform for a 7-phase inverter in sector 1

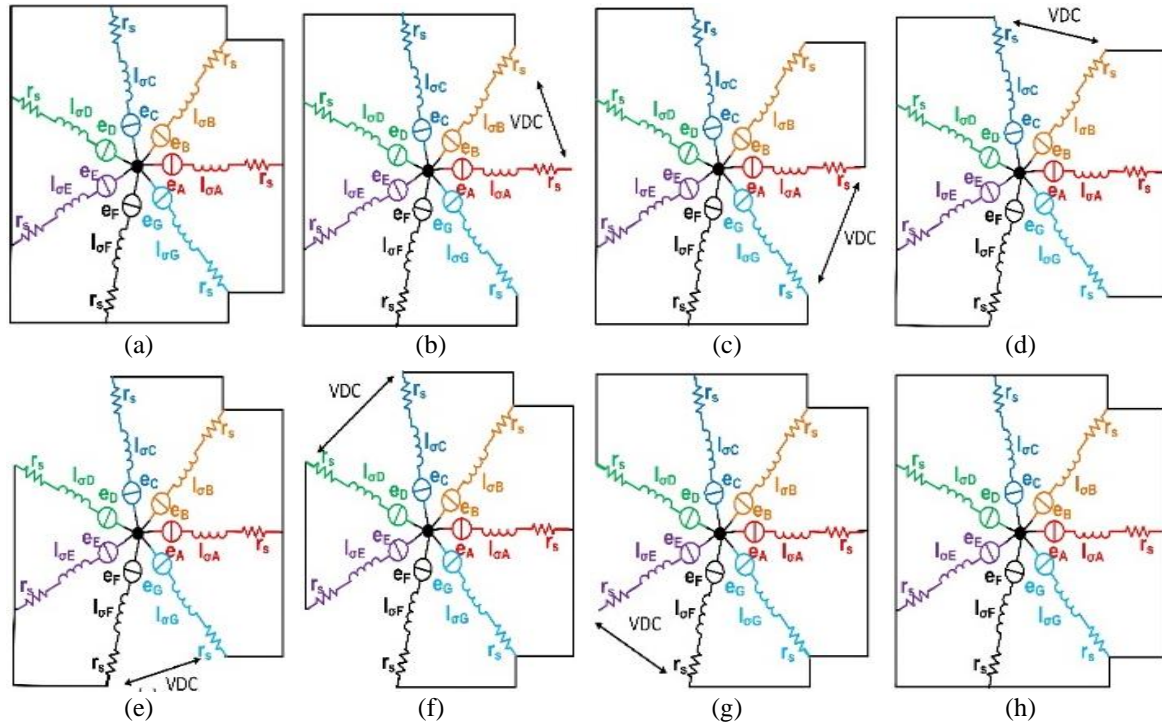


Figure 9. Dynamic equivalent of the 7-phase PMSM during generating different vectors one PWM period (a) V0 is generated, (b) V1 is generated, (c) V3 is generated, (d) V67 is generated, (e) V71 is generated, (f) V103 is generated, (g) V111 is generated, and (h) V127 is generated

Table 3. Estimated position signals in each sector of the 7-phase PMSM

Sector no	PsA=q()	PsB=q()	PsC=q()	PsD=q()	PsE=q()	PsF=q()	PsG=q()
1	$i_{sA}^{H2} - i_{sA}^{H1}$	$i_{sB}^{H2} - i_{sB}^{H1}$	$i_{sC}^{H4} - i_{sC}^{H3}$	$i_{sD}^{H6} - i_{sD}^{H5}$	$i_{sE}^{H7} - i_{sE}^{H6}$	$i_{sF}^{H5} - i_{sF}^{H4}$	$i_{sG}^{H3} - i_{sG}^{H2}$
2	$i_{sA}^{H2} - i_{sA}^{H1}$	$i_{sB}^{H1} - i_{sB}^{H0}$	$i_{sC}^{H3} - i_{sC}^{H2}$	$i_{sD}^{H5} - i_{sD}^{H4}$	$i_{sE}^{H7} - i_{sE}^{H6}$	$i_{sF}^{H6} - i_{sF}^{H5}$	$i_{sG}^{H4} - i_{sG}^{H3}$
3	$i_{sA}^{H3} - i_{sA}^{H2}$	$i_{sB}^{H1} - i_{sB}^{H0}$	$i_{sC}^{H2} - i_{sC}^{H1}$	$i_{sD}^{H4} - i_{sD}^{H3}$	$i_{sE}^{H6} - i_{sE}^{H5}$	$i_{sF}^{H7} - i_{sF}^{H6}$	$i_{sG}^{H5} - i_{sG}^{H4}$
4	$i_{sA}^{H4} - i_{sA}^{H3}$	$i_{sB}^{H2} - i_{sB}^{H1}$	$i_{sC}^{H1} - i_{sC}^{H0}$	$i_{sD}^{H3} - i_{sD}^{H2}$	$i_{sE}^{H5} - i_{sE}^{H4}$	$i_{sF}^{H7} - i_{sF}^{H6}$	$i_{sG}^{H6} - i_{sG}^{H5}$
5	$i_{sA}^{H5} - i_{sA}^{H4}$	$i_{sB}^{H3} - i_{sB}^{H2}$	$i_{sC}^{H1} - i_{sC}^{H0}$	$i_{sD}^{H2} - i_{sD}^{H1}$	$i_{sE}^{H4} - i_{sE}^{H3}$	$i_{sF}^{H6} - i_{sF}^{H5}$	$i_{sG}^{H7} - i_{sG}^{H6}$
6	$i_{sA}^{H6} - i_{sA}^{H5}$	$i_{sB}^{H4} - i_{sB}^{H3}$	$i_{sC}^{H2} - i_{sC}^{H1}$	$i_{sD}^{H1} - i_{sD}^{H0}$	$i_{sE}^{H3} - i_{sE}^{H2}$	$i_{sF}^{H5} - i_{sF}^{H4}$	$i_{sG}^{H7} - i_{sG}^{H6}$
7	$i_{sA}^{H7} - i_{sA}^{H6}$	$i_{sB}^{H5} - i_{sB}^{H4}$	$i_{sC}^{H3} - i_{sC}^{H2}$	$i_{sD}^{H1} - i_{sD}^{H0}$	$i_{sE}^{H2} - i_{sE}^{H1}$	$i_{sF}^{H4} - i_{sF}^{H3}$	$i_{sG}^{H6} - i_{sG}^{H5}$
8	$i_{sA}^{H7} - i_{sA}^{H6}$	$i_{sB}^{H6} - i_{sB}^{H5}$	$i_{sC}^{H4} - i_{sC}^{H3}$	$i_{sD}^{H2} - i_{sD}^{H1}$	$i_{sE}^{H1} - i_{sE}^{H0}$	$i_{sF}^{H3} - i_{sF}^{H2}$	$i_{sG}^{H5} - i_{sG}^{H4}$
9	$i_{sA}^{H6} - i_{sA}^{H5}$	$i_{sB}^{H7} - i_{sB}^{H6}$	$i_{sC}^{H5} - i_{sC}^{H4}$	$i_{sD}^{H3} - i_{sD}^{H2}$	$i_{sE}^{H1} - i_{sE}^{H0}$	$i_{sF}^{H2} - i_{sF}^{H1}$	$i_{sG}^{H4} - i_{sG}^{H3}$
10	$i_{sA}^{H5} - i_{sA}^{H4}$	$i_{sB}^{H7} - i_{sB}^{H6}$	$i_{sC}^{H6} - i_{sC}^{H5}$	$i_{sD}^{H4} - i_{sD}^{H3}$	$i_{sE}^{H2} - i_{sE}^{H1}$	$i_{sF}^{H1} - i_{sF}^{H0}$	$i_{sG}^{H3} - i_{sG}^{H2}$
11	$i_{sA}^{H4} - i_{sA}^{H3}$	$i_{sB}^{H6} - i_{sB}^{H5}$	$i_{sC}^{H7} - i_{sC}^{H6}$	$i_{sD}^{H5} - i_{sD}^{H4}$	$i_{sE}^{H3} - i_{sE}^{H2}$	$i_{sF}^{H1} - i_{sF}^{H0}$	$i_{sG}^{H2} - i_{sG}^{H1}$
12	$i_{sA}^{H3} - i_{sA}^{H2}$	$i_{sB}^{H5} - i_{sB}^{H4}$	$i_{sC}^{H7} - i_{sC}^{H6}$	$i_{sD}^{H6} - i_{sD}^{H5}$	$i_{sE}^{H4} - i_{sE}^{H3}$	$i_{sF}^{H2} - i_{sF}^{H1}$	$i_{sG}^{H1} - i_{sG}^{H0}$
13	$i_{sA}^{H2} - i_{sA}^{H1}$	$i_{sB}^{H4} - i_{sB}^{H3}$	$i_{sC}^{H6} - i_{sC}^{H5}$	$i_{sD}^{H7} - i_{sD}^{H6}$	$i_{sE}^{H5} - i_{sE}^{H4}$	$i_{sF}^{H3} - i_{sF}^{H2}$	$i_{sG}^{H1} - i_{sG}^{H0}$
14	$i_{sA}^{H1} - i_{sA}^{H0}$	$i_{sB}^{H3} - i_{sB}^{H2}$	$i_{sC}^{H5} - i_{sC}^{H4}$	$i_{sD}^{H7} - i_{sD}^{H6}$	$i_{sE}^{H6} - i_{sE}^{H5}$	$i_{sF}^{H4} - i_{sF}^{H3}$	$i_{sG}^{H2} - i_{sG}^{H1}$

4. SIMULATION RESULTS

4.1. Saliency position tracking

The proposed algorithm given in Table 3 to get the shaft position and speed of the 7-phase drive when a failure in a speed sensor is occurred is simulated in SABER based on the control scheme shown in Figure 10. The stator currents derivatives (i_{sA} , i_{sB} , i_{sC} , i_{sD} , i_{sE} , i_{sF} , and i_{sG}) of the motor were measured and the scalar position signals (Palfa, and Pbeta) were constructed as (22-23) and Table 3. Then a mechanical observer [29] was utilized to enhance the quality of the estimated position signals by removing the noises. Note the simulation includes a minimum pulse width of 10us when the rate of change of the motors currents was sampled.

The results provided by simulating the control structure illustrated in Figure 10 in the SABER simulator are depicted in the Figure 11. The speed command of the speed controller was set to 180 rpm while the motor operating at full load condition. Then, the speed command of the speed controller was changed to 0 and to 180 rpm at times 1.5 s and 3 s respectively. The simulation results demonstrate that the motor measured speed tracked the speed command of the speed controller effectively with good transient and steady-state errors. Moreover, the results demonstrate the algorithm developed in this paper was succeeded in extracting the rotor position and speed at low and zero speeds.

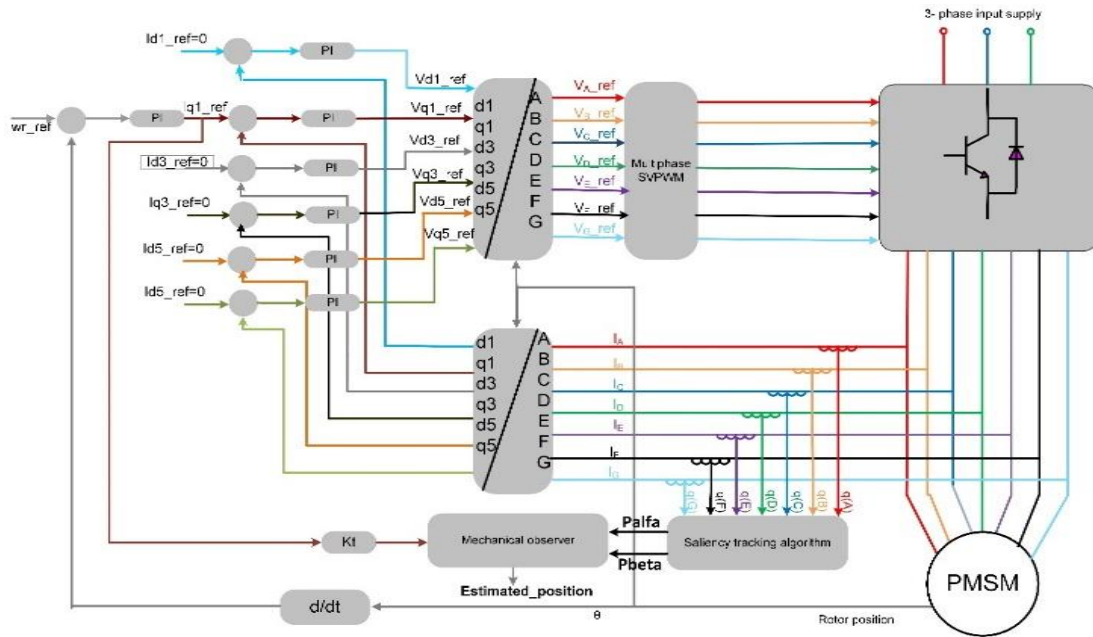


Figure 10. Control structure of the 7-phase drive to estimate the shaft speed and position

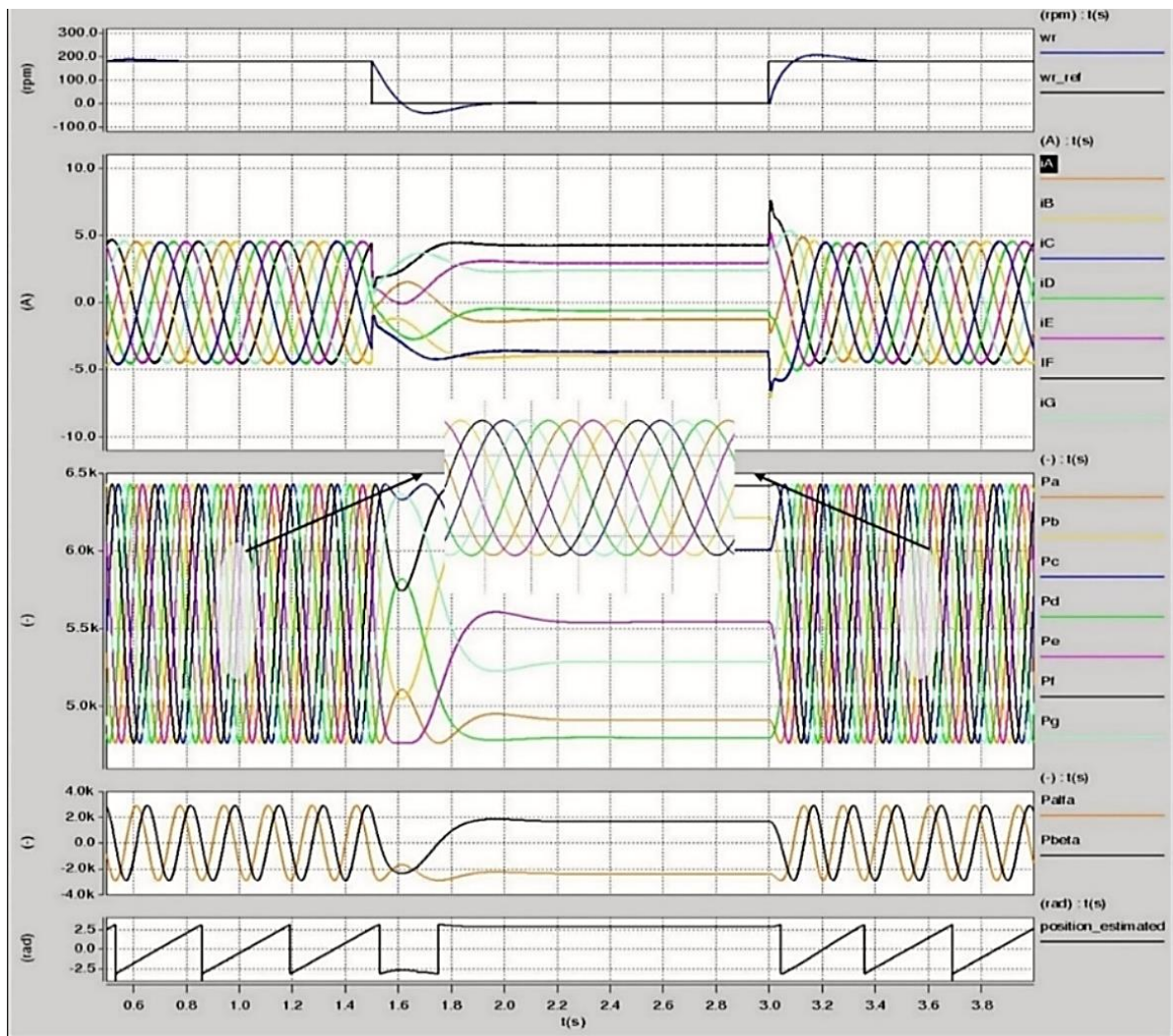


Figure 11. Saliency tracking results

4.2. Control of the 7-phase drive in the case of a failure in speed sensor

The schematic of the control structure of the 7-phase drive when a failure in the speed sensor is occurred has been simulated using the SABER simulator. The algorithm developed in this research besides the mechanical observer was used to get the shaft position and the speed of the motor when a failure in the speed sensor is occurred. Then these signals are utilized to achieve sensorless speed-controlled 7-phase PMSM drive as shown in Figure 12.

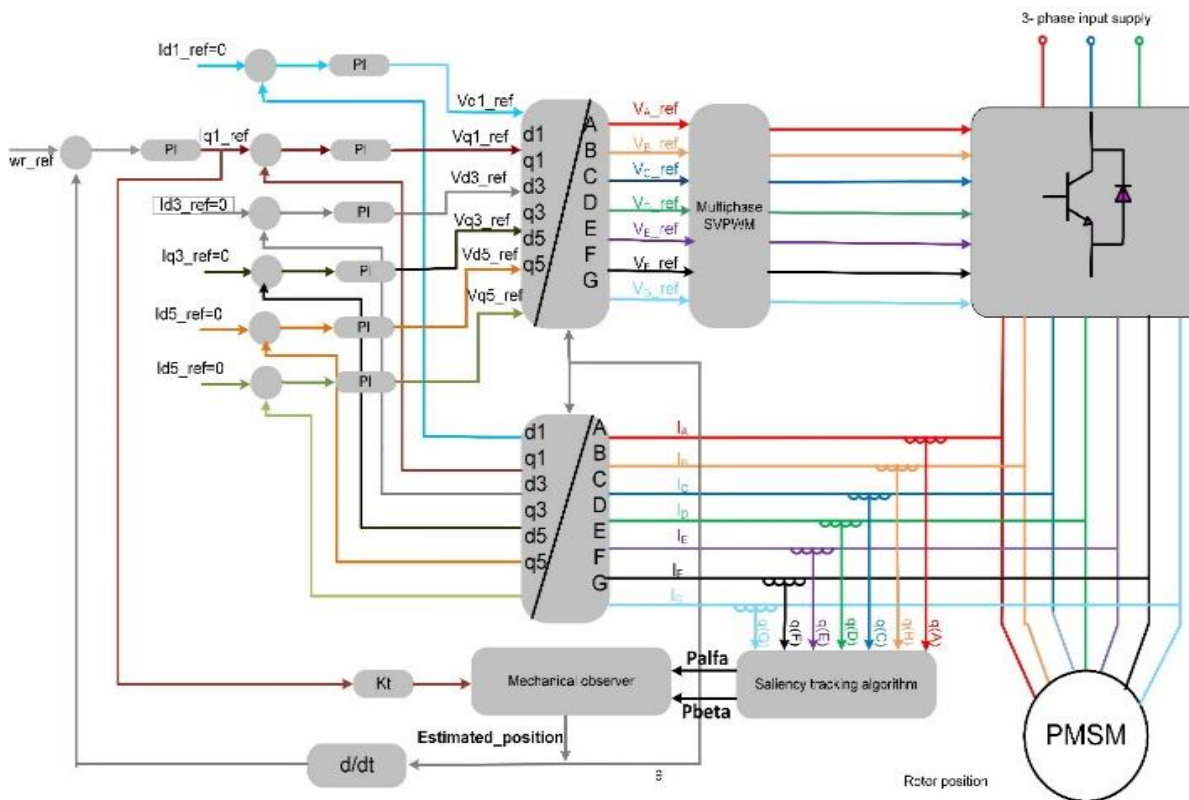


Figure 12. Sensorless speed-controlled 7-phase drive

Figure 13 shows the simulation results for a speed-controlled 7-phase motor in the case of a failure in the speed sensor. The speed command of the speed controller was set to 30 rpm and at full load. Then at $t=3$ s, the speed command of the speed controller was modified to 0 rpm. Finally, at $t=5$ s the speed command of the speed controller was modified to -30 rpm. The results depicted in Figure 13 demonstrate the excellent dynamic and steady-state response of the whole drive system to the low-speed steps command in the case of a failure in the speed sensor.

Figure 14 shows similar results that were given in Figure 13 but at a higher speed steps command. The speed command of the speed controller of the 7-phase motor drive was set to 300 rpm at full load in the case of a failure in the speed sensor. At $t=2$ s, the speed command of the speed controller was changed from 300 rpm to 0 rpm. then at $t=3.5$ s, the speed command of the speed controller was changed to 300 rpm again. The results demonstrate the excellent response of the whole drive system to the high-speed steps command in the case of a failure in the speed sensor.

Figure 15 illustrates the stability of the 7-phase drive in the case of a failure in the speed sensor when a load disturbance was applied at low speed (100 rpm). The speed command of the speed controller of the 7-phase motor was set to 100 rpm at 20% of the rated load. Then the load on the motor was increased instantly to 80% of the full load at $t=1$ s. at $t=2$ s, and the load on the motor was decreased instantly to 20% of the full load. After that, at $t=3$ s, the speed command of the speed controller was set to 0 rpm. Then it was set to -100 rpm at $t=5$ s. Finally, the load on the motor was increased instantly to 80% of the full load at $t=6$ s and decreased instantly to 20% at $t=6$ s. all these steps in the load and speed were done in the case of a failure in the speed sensor. The results show that the system maintained the speed in all the cases.

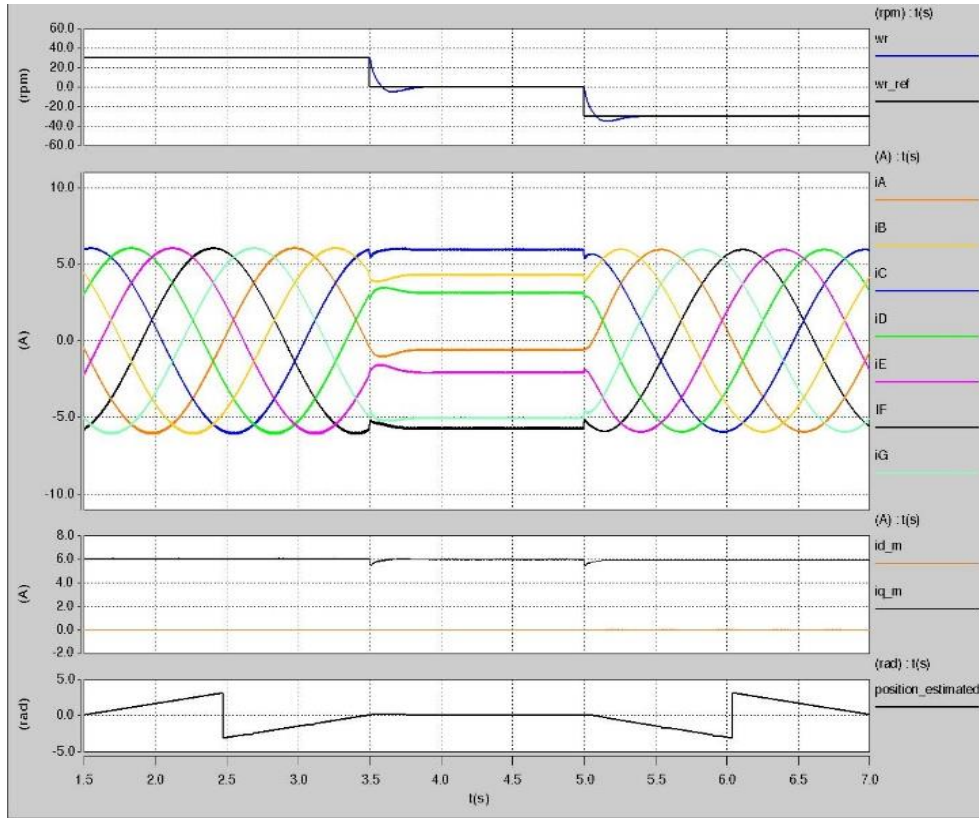


Figure 13. Low-speed operation of the 7-phase motor in the case of a failure in the speed sensor

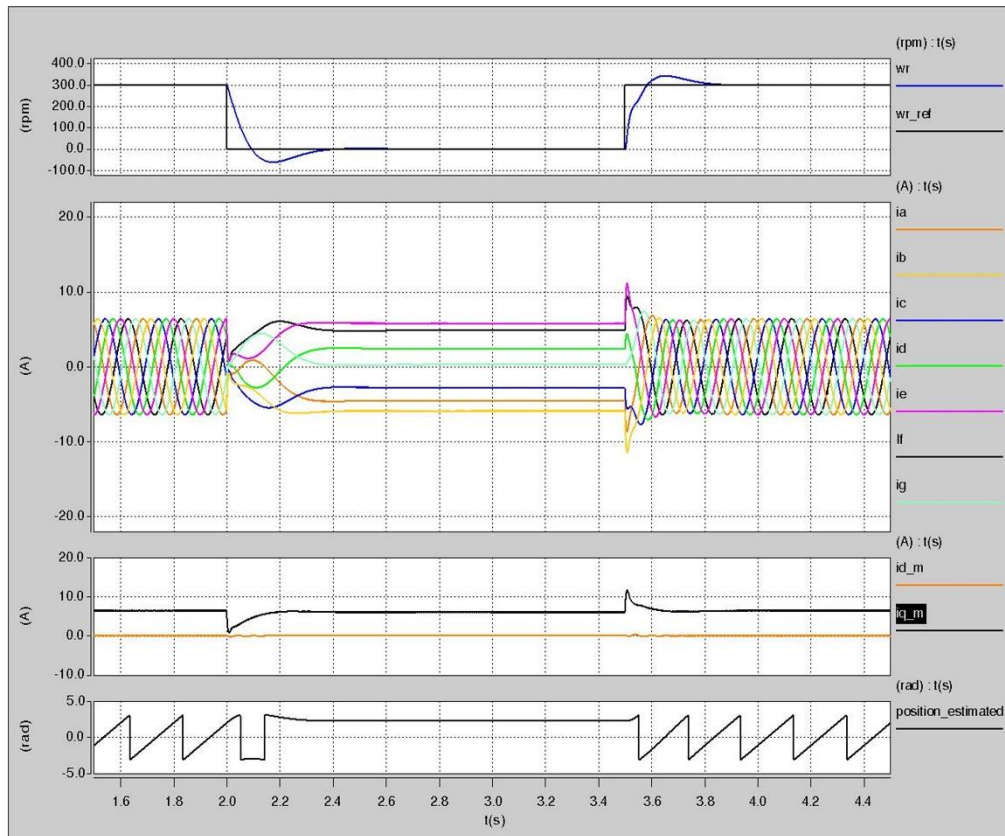


Figure 14. High-speed operation of the 7-phase motor in the case of a failure in the speed sensor

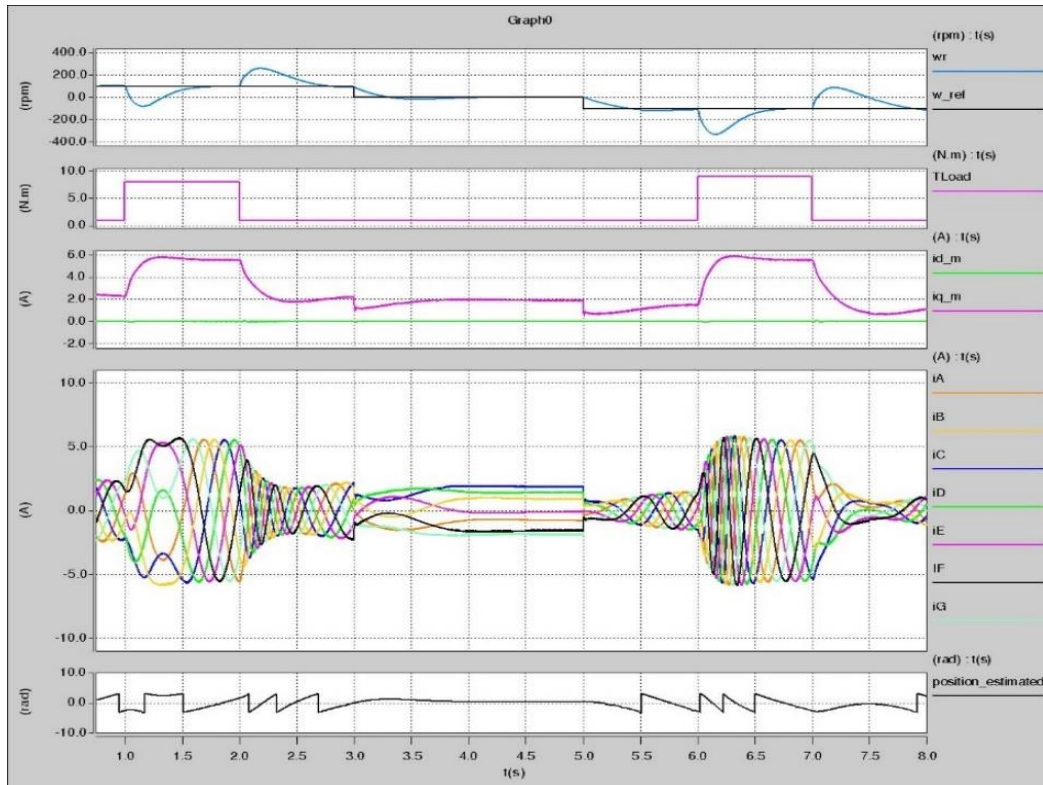


Figure 15. Load steps operation of the 7-phase motor in the case of a failure in the speed sensor

5. CONCLUSION

This paper has presented a new control technique of the 7-phase PMSM drive system in the case of a failure in the speed sensor. This control technique is based on obtaining the rotor position and speed in the case of a failure by tracking the saliency position of the 7-phase PMSM motor using multi-dimension SVPWM techniques. The results have shown the enhanced robustness of the whole drive system at operating conditions. The implementation of this technique is easy and can be applied to the induction motor also.




REFERENCES

- [1] M. Villani, M. Tursini, G. Fabri, and L. Castellini, "Multi-phase fault tolerant drives for aircraft applications," in *Electrical Systems for Aircraft, Railway and Ship Propulsion*, Oct. 2010, pp. 1–6, doi: 10.1109/ESARS.2010.5665246.
- [2] Q. Song, X. Zhang, F. Yu, and C. Zhang, "Research on space vector PWM of five-phase three-level inverter," in *2005 International Conference on Electrical Machines and Systems*, 2005, pp. 1418–1421, doi: 10.1109/ICEMS.2005.202782.
- [3] G. Grandi, G. Serra, and A. Tani, "Space vector modulation of a seven-phase voltage source inverter," in *International Symposium on Power Electronics, Electrical Drives, Automation and Motion, 2006. SPEEDAM 2006.*, 2006, pp. 1149–1156, doi: 10.1109/SPEEDAM.2006.1649941.
- [4] J. Pradeep and R. Devanathan, "Comparative analysis and simulation of PWM and SVPWM inverter fed permanent magnet synchronous motor," in *2012 International Conference on Emerging Trends in Electrical Engineering and Energy Management (ICETEEEM)*, Dec. 2012, pp. 299–305, doi: 10.1109/ICETEEEM.2012.6494517.
- [5] D. Casadei, D. Dujic, E. Levi, G. Serra, A. Tani, and L. Zarri, "General modulation strategy for seven-phase inverters with independent control of multiple voltage space vectors," *IEEE Transactions on Industrial Electronics*, vol. 55, no. 5, pp. 1921–1932, May 2008, doi: 10.1109/TIE.2008.918481.
- [6] D. Zhang, B. Xu, H. Yang, and P. Zhu, "Simulation analysis of SVPWM based on seven-phase permanent magnet synchronous motor," in *2017 International Conference on Control, Automation and Information Sciences (ICCAIS)*, Oct. 2017, pp. 251–256, doi: 10.1109/ICCAIS.2017.8217585.
- [7] W. Gong, Y. Wang, Z. Cai, and L. Wang, "Finding multiple roots of nonlinear equation systems via a repulsion-based adaptive differential evolution," *IEEE Transactions on Systems, Man, and Cybernetics: Systems*, vol. 50, no. 4, pp. 1499–1513, Apr. 2020, doi: 10.1109/TSMC.2018.2828018.
- [8] S. M. Dabour, "Space vector PWM technique to reduce common mode voltage for seven-phase inverters," *Small*, vol. 905, no. 2, pp. 1–7, 2017.
- [9] M. Lu, D. Zhang, B. Xu, H. Yang, and Y. Xin, "Multiphase SVPWM strategy analysis and implementation of seven-phase permanent magnet synchronous motor," *Complexity*, vol. 2020, pp. 1–12, Oct. 2020, doi: 10.1155/2020/8854472.
- [10] J. J. Listwan, "Analysis of fault states in drive systems with multi-phase induction motors," *Archives of Electrical Engineering*, vol. 68, no. 4, pp. 817–830, 2019, doi: 10.24425/ae.2019.130685.
- [11] K. Klimkowski and M. Dybkowski, "A fault tolerant control structure for an induction motor drive system," *Automatika*, vol. 57,




- no. 3, pp. 638–647, Jan. 2016, doi: 10.7305/automatika.2017.02.1642.
- [12] M. Dybkowski, K. Klimkowski, and T. O. -Kowalska, "Speed and current sensor fault-tolerant-control of the induction motor drive," in *Advanced Control of Electrical Drives and Power Electronic Converters*, Cham: Springer, 2017, pp. 141–167, doi: 10.1007/978-3-319-45735-2_7.
- [13] M. Dybkowski, K. Klimkowski, and T. O. -Kowalska, "Speed sensor fault tolerant direct torque control of induction motor drive," in *2014 16th International Power Electronics and Motion Control Conference and Exposition*, Sep. 2014, pp. 679–684, doi: 10.1109/EPEPEMC.2014.6980574.
- [14] S. Bednarz and M. Dybkowski, "Induction motor windings faults detection using flux-error based MRAS estimators," *Diagnostyka*, vol. 20, no. 2, pp. 87–96, May 2019, doi: 10.29354/diag/109092.
- [15] M. Korzonek, G. Tarchala, and T. O. -Kowalska, "A review on MRAS-type speed estimators for reliable and efficient induction motor drives," *ISA Transactions*, vol. 93, pp. 1–13, Oct. 2019, doi: 10.1016/j.isatra.2019.03.022.
- [16] L. Zheng, J. E. Fletcher, B. W. Williams, and X. He, "A novel direct torque control scheme for a sensorless five-phase induction motor drive," *IEEE Transactions on Industrial Electronics*, vol. 58, no. 2, pp. 503–513, Feb. 2011, doi: 10.1109/TIE.2010.2047830.
- [17] L. Zhang, Y. Fan, C. Li, A. Nied, and M. Cheng, "Fault-tolerant sensorless control of a five-phase FTFSCW-IPM motor based on a wide-speed strong-robustness sliding mode observer," *IEEE Transactions on Energy Conversion*, vol. 33, no. 1, pp. 87–95, Mar. 2018, doi: 10.1109/TEC.2017.2727074.
- [18] A. H. Almarhoon, Z. Q. Zhu, and P. Xu, "Improved rotor position estimation accuracy by rotating carrier signal injection utilizing zero-sequence carrier voltage for dual three-phase PMSM," *IEEE Transactions on Industrial Electronics*, vol. 64, no. 6, pp. 4454–4462, Jun. 2017, doi: 10.1109/TIE.2016.2561261.
- [19] G. Liu, C. Geng, and Q. Chen, "Sensorless control for five-phase IPMSM drives by injecting HF square-wave voltage signal into third harmonic space," *IEEE Access*, vol. 8, pp. 69712–69721, 2020, doi: 10.1109/ACCESS.2020.2986347.
- [20] K. Saleh and M. Sumner, "Sensorless speed control of five-phase PMSM drives in case of a single-phase open-circuit fault," *Iranian Journal of Science and Technology, Transactions of Electrical Engineering*, vol. 43, no. 3, pp. 501–517, Sep. 2019, doi: 10.1007/s40998-018-00173-4.
- [21] E. Z. M. Salem, "Speed sensorless control of seven phase asynchronous motor drive system using extended Kalman filter," *International Journal of Electronics Letters*, vol. 10, no. 2, pp. 144–160, Apr. 2022, doi: 10.1080/21681724.2020.1870720.
- [22] A. Bıçak and A. Gelen, "Sensorless direct torque control based on seven-level torque hysteresis controller for five-phase IPMSM using a sliding-mode observer," *Engineering Science and Technology, an International Journal*, vol. 24, no. 5, pp. 1134–1143, Oct. 2021, doi: 10.1016/j.jestch.2021.02.004.
- [23] J. Listwan and K. Pienkowski, "Comparison of DFOC of seven-phase induction motor with PI and fuzzy-logic speed controller under speed sensor fault," *Przegląd Elektrotechniczny*, vol. 1, no. 10, pp. 11–15, Oct. 2020, doi: 10.15199/48.2020.10.02.
- [24] Y.-C. Luo and W.-A. Huang, "Sensorless rotor field direct orientation controlled induction motor drive with particle swarm optimization algorithm flux observer," *Journal of Low Frequency Noise, Vibration and Active Control*, vol. 38, no. 2, pp. 692–705, Jun. 2019, doi: 10.1177/1461348418824942.
- [25] M. A. Mossa, H. Echeikh, A. Iqbal, T. D. Do, and A. S. A. -Sumaiti, "A novel sensorless control for multiphase induction motor drives based on singularly perturbed sliding mode observer-experimental validation," *Applied Sciences*, vol. 10, no. 8, p. 2776, Apr. 2020, doi: 10.3390/app10082776.
- [26] J. Listwan and K. Pieńkowski, "Comparative analysis of control methods with model reference adaptive system estimators of a seven-phase induction motor with encoder failure," *Energies*, vol. 14, no. 4, p. 1147, Feb. 2021, doi: 10.3390/en14041147.
- [27] Y. Mini, N. K. Nguyen, and E. Semail, "A novel sensorless control strategy based on sliding mode observer for non-sinusoidal seven-phase PMSM," in *The 10th International Conference on Power Electronics, Machines and Drives (PEMD 2020)*, 2021, pp. 694–699, doi: 10.1049/icp.2021.1120.
- [28] K. Saleh and M. Sumner, "Sensorless control of seven-phase PMSM drives using NSV-SVPWM with minimum current distortion," *Electronics*, vol. 11, no. 5, p. 792, Mar. 2022, doi: 10.3390/electronics11050792.
- [29] R. D. Lorenz and K. W. V. Patten, "High-resolution velocity estimation for all-digital, AC servo drives," *IEEE Transactions on Industry Applications*, vol. 27, no. 4, pp. 701–705, 1991, doi: 10.1109/28.85485.

BIOGRAPHIES OF AUTHORS



Kamel Saleh    was born in Tulkarm, Palestine, in 1980. He received the B.E. degree in electrical engineering from An-Najah National University in 2003. From 2003 to 2005, he worked as a planning engineer with the Palestinian Energy Authority. In 2005, He joined Nottingham University as a graduate student and obtained a master degree and Ph.D degree in electrical engineering in 2006 and 2009 respectively. From 2009 to 2010, he worked as a researcher with as a power electronics, control, and machine (PEMC) group at Nottingham university. Finally, in 2010 he joined the department of electrical engineering at An-Najah National university as a lecturer. Finally, in 2018 he was promoted to be associated professor. His current researches include sensorless control of multi-phase drive, multilevel inverters drive, DSTATCOM and renewable energy. He can be contacted at email: kamel.saleh@najah.edu.



Mark Sumner    received the B. Eng degree in Electrical and Electronic Engineering from Leeds University in 1986 and then worked for Rolls Royce Ltd in Ansty, UK. Moving to the University of Nottingham. He completed his Ph.D in induction motor drives in 1990, and after working as a research assistant, was appointed Lecturer in October 1992. He is now Professor of Electrical Energy Systems. His research interests cover control of power electronic systems including sensorless motor drives, diagnostics and prognostics for drive systems, power electronics for enhanced power quality and novel power system fault location strategies. He can be contacted at email: mark.sumner@nottingham.ac.uk.